Electronic Supplementary Material (ESI) for Soft Matter.

Supplementary Information

Towards Mechanical Characterization of Granular Biofilms by Optical Coherence Elastography Measurements of Circumferential Elastic Waves

Hong-Cin Liou[1], Fabrizio Sabba[2], Aaron I. Packman[2], Alex Rosenthal[2], George Wells[2], Oluwaseyi Balogun[1,2]*

[1]Mechanical Engineering Department, Northwestern University, Evanston, IL 60208

[2]Civil and Environmental Engineering Department, Northwestern University, Evanston, IL 60208

***Corresponding author:**

Oluwaseyi Balogun, Phone: +1 847-491-3054; e-mail: o-balogun@u.northwestern.edu

The following are included as supporting information for this paper:

Number of pages: 8

Number of supplementary sections: 3

Number of figures: 2

Number of tables: 1

S1 – Locating local minima in the (ω,k) space for the solutions of the characteristic equation

The complex characteristic equation det(**S**) = 0 (eqn 29) was solved by searching the solution pairs of angular frequency $\omega = 2\pi f$ (f is frequency) and complex wavenumber k where the magnitude for the left-hand side of eqn (29) equals to zero, i.e., |det(**S**)| = 0. Note that it may be difficult to obtain absolute zero in numerical calculation; therefore, in practice, the solutions were determined instead by locating local minima of |det(**S**)| in the (ω,k) space. Specifically, the search of solutions includes the following steps: (1) choose a certain angular frequency ω within the range of interest, (2) sweep a range of k to find the local minima, and (3) change to a different ω and repeat step (2). For pure-elastic materials, the wavenumber k only has the real part, so the sweep in step (2) was one-dimensional along the axis of real wavenumbers $k^R = \mathrm{Re}\{k\}$. For viscoelastic materials, k is a complex number composed of the real (k^R) and imaginary ($k^I = \mathrm{Im}\{k\}$) parts, so the sweep became two-dimensional over the (k^R,k^I) plane.

Figure S1a shows an example of |det(**S**)| variation over the (k^R,k^I) space for a model viscoelastic material. The magnitude |det(**S**)| is plotted in logarithmic scale for visualization purposes. The dent in the middle of the surface is one of the local minima of |det(**S**)|, and the wavy wrinkles on the upper and lower sides of the surface are numerical errors. The wave wrinkles were confirmed to be numerical errors since they were also observed in the pure-elastic model material as shown in Fig. S1b. The pure-elastic material had the same properties as the viscoelastic material with the sole difference that the shear viscosity η_μ was changed to zero. Since the wavenumber for the pure-elastic material only has the real part, the local minima should only appear on the $k^I = 0$ axis.

To remove the numerical errors and identify the local minimum in Fig. S1a, |det(**S**)| of the pure-elastic material (Fig. S1b) was subtracted from that of the viscoelastic material (Fig. S1a), yielding a clear inverted cone indicating the local minimum as shown in Fig. S2.

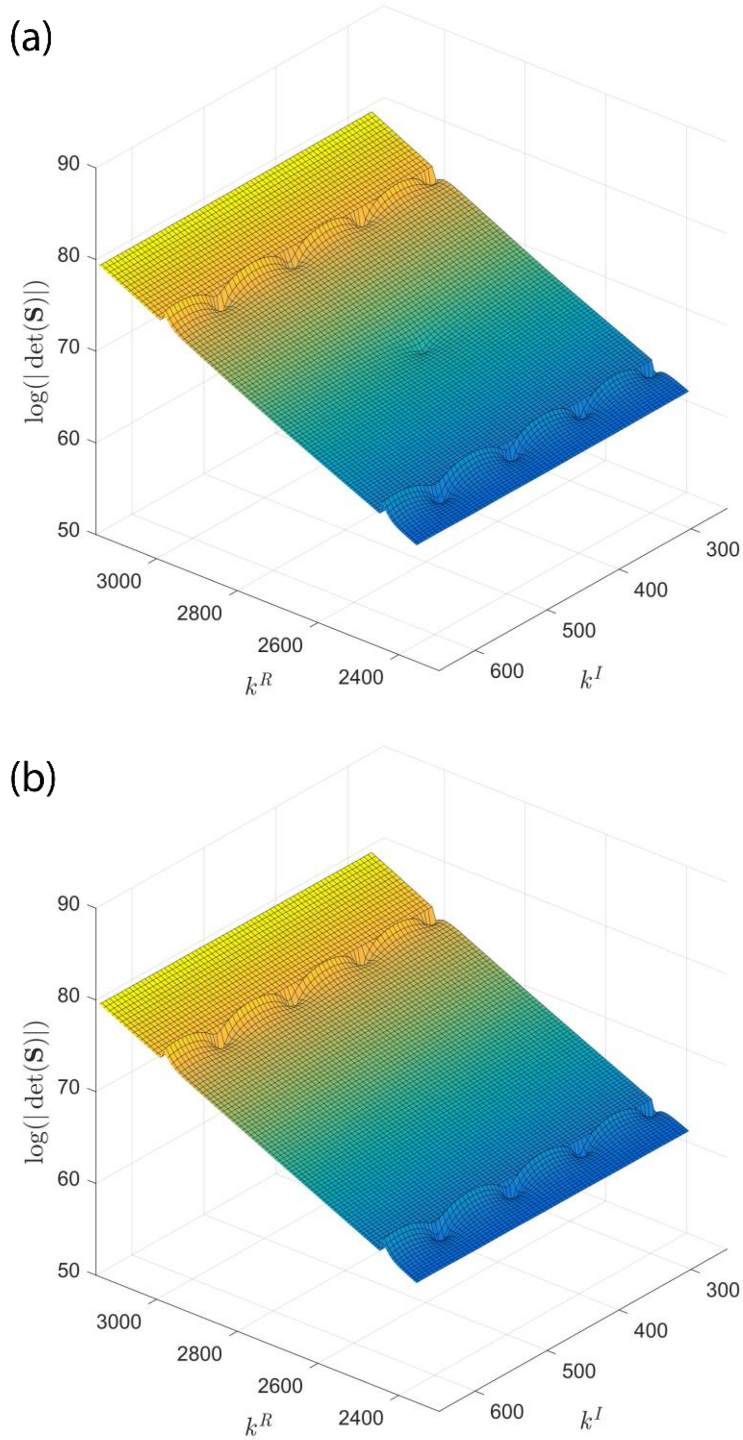

Fig. S1: Variation of the magnitude |det(**S**)| over the (k^R,k^I) plane for model materials with (a) viscoelastic properties and (b) pure-elastic properties. The wavy wrinkles observed both in (a) and (b), suggest that they are numerical errors.

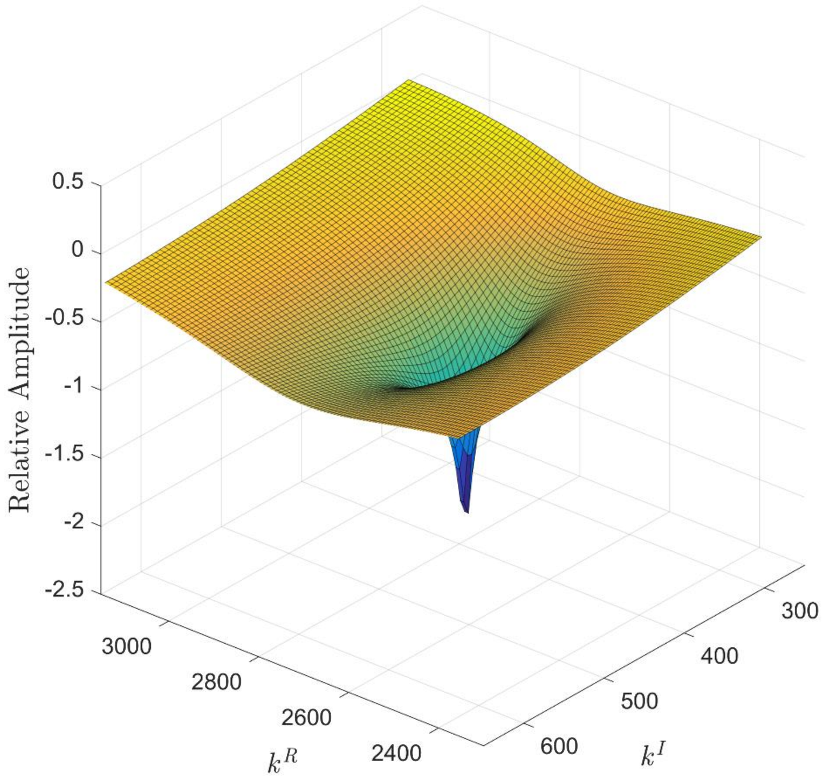

Fig. S2: Local minimum of |det(**S**)| obtained by subtracting the |det(**S**)| of the pure-elastic material (Fig. S1b) from that of the viscoelastic material (Fig. S1a).

S2 – Simplified Characteristic Equation for the Elastic Curved Plate Reported in Liu and Qu (1998)

The elastic curved plate reported in the article has traction-free condition for both sides of the plate, which corresponds to four boundary conditions: zero normal traction at the inner surface (r = a) $\sigma_{rr}|_{r=a} = 0$, , zero normal traction at the outer surface (r = b), $\sigma_{rr}|_{r=b} = 0$, zero shear traction at the inner surface, $\sigma_{r\theta}|_{r=a} = 0$, and zero shear traction at the outer surface, $\sigma_{r\theta}|_{r=b} = 0$. These conditions lead to a four-by-four **S** matrix in eqn (28):

$$\mathbf{S} = \begin{bmatrix} D_{31}|_{r=a} & D_{32}|_{r=a} & D_{33}|_{r=a} & D_{34}|_{r=a} \\ D_{31}|_{r=b} & D_{32}|_{r=b} & D_{33}|_{r=b} & D_{34}|_{r=b} \\ D_{41}|_{r=a} & D_{42}|_{r=a} & D_{43}|_{r=a} & D_{44}|_{r=a} \\ D_{41}|_{r=b} & D_{42}|_{r=b} & D_{43}|_{r=b} & D_{44}|_{r=b} \end{bmatrix} \quad \text{(S7)}$$

S3 – Numerical methods for calculating Bessul functions with complex orders

In eqn (14) and (15), the general solutions of the scalar and vector potential functions are linear superpositions of Bessel functions with a complex order $\nu = kb$ as k is the complex wavenumber. A numerical challenge arises with the Bessel functions that have complex orders since they are not supported in MATLAB (Release R2016b, MathWorks). To resolve the challenge, this section provides the details of mathematical properties that enable the calculation of the approximate values for Bessel functions of this kind.

According to eqn (9.1.20) in *Handbook of Mathematical Functions with Formulas, Graphs, and Mathematical Tables* (Abramowitz and Stegun, 1964), the Bessel function of the first kind has the expression:

$$J_\nu(z) = \frac{2\left(\frac{1}{2}z\right)^\nu}{\sqrt{\pi}\,\Gamma\left(\nu+\frac{1}{2}\right)} \int_0^1 (1-t^2)^{\nu-\frac{1}{2}} \cos(zt)\, dt, \;\; \mathbb{R}(\nu) > -\frac{1}{2} \tag{S1}$$

where ν and z are the order and the argument, respectively, of the Bessel function J, and $\Gamma(x)$ is the Gamma function. In our case, the order ν is the product of the complex wavenumber k and outer sphere radius b, i.e., $\nu = kb$, so that ν is complex.

The recurrence relation (eqn 9.1.27 in Abramowitz and Stegun) can be used to extend the order of the Bessel function to the whole complex plane that is not covered in eqn (S1); i.e., use

$$J_{\nu-1}(z) + J_{\nu+1}(z) = \frac{2\nu}{z} J_\nu(z) \tag{S2}$$

for $\mathbb{R}(\nu) \leq -1/2$.

In addition, the Bessel function of the second kind $Y_\nu(z)$ is also required in our theoretical model, which has the relationship with the first kind (eqn 9.1.2 in Abramowitz and Stegun) given by

$$Y_\nu(z) = \frac{J_\nu(z)\cos(\nu\pi) - J_{-\nu}(z)}{\sin(\nu\pi)} \tag{S3}$$

Note that the Gamma function in eqn (S1) has a complex argument $\nu + 1/2$; therefore, the value of Gamma function must be determined through the definition of integral form (6.1.1 in Abramowitz and Stegun):

$$\Gamma(x) = \int_0^\infty t^{x-1} e^{-t} dt\,,\ \mathbb{R}(x) > 0 \tag{S4}$$

Eqn (S4) can be calculated using the Upper Incomplete Gamma Function `igamma` provided in MATLAB function library; however, the calculation speed of this approximation might be slow. An alternative method with enhanced calculation speed to acquire the approximate values of the Gamma function with complex argument can be found in an algorithm library created by Paul Godfrey (http://my.fit.edu/~gabdo/paulbio.html).

Similar to the Bessel functions, the recurrence relation of the Gamma function (eqn 6.1.15 in Abramowitz and Stegun) can be used to extend the argument of the Gamma function to the whole complex plane that is not covered in eqn (S4); i.e., use

$$\Gamma(x+1) = x\Gamma(x) \tag{S5}$$

for $\mathbb{R}(x) \leq 0$.

With eqn (S1) to (S5), the Hankel function of the first kind that represents the waves propagating along the positive *r*-direction can be obtained by the relationship with the Bessel functions:

$$H_\nu^{(1)}(z) = J_\nu(z) + iY_\nu(z) \tag{S6}$$

Hence, all required functions are defined.

To validate the two aforementioned approximations of Gamma function (Upper Incomplete Gamma Function `igamma` in MATLAB function library and the program created by Godfrey), Bessel functions $J_\nu(z)$ and $Y_\nu(z)$ with different complex orders ν and real arguments z were calculated and compared to the values reported in a reference (K. L. J. Fong, *A Study of Curvature Effects on Guided Elastic Waves*, Ph.D. thesis of Imperial College London, pp. 148). The comparison is demonstrated in Table S1, and the results show both approximations have at least 10 digits of precision compared to the reference.

$J_\nu(z)$ with $\nu = 30 + 50i$			
z	Reference	MATLAB `igamma`	Godfrey
70	−5.93644837574622 × 10^{23} −6.21989546226278 × $10^{23}i$	**−5.93644837574**486 × 10^{23} **−6.21989546226**806 × $10^{23}i$	**−5.93644837574**481 × 10^{23} **−6.21989546226**825 × $10^{23}i$
31	9.38713109974277 × 10^{15} −2.04157148369613 × $10^{15}i$	**9.387131099742**98 × 10^{15} **−2.04157148369613** × $10^{15}i$	**9.38713109974**313 × 10^{15} **−2.04157148369**597 × $10^{15}i$
30	−1.95359736621662 × 10^{15} −3.54953866450241 × $10^{15}i$	**−1.9535973662166**3 × 10^{15} **−3.549538664502**50 × $10^{15}i$	**−1.953597366216**59 × 10^{15} **−3.549538664502**58 × $10^{15}i$
10	−102.750648203869 +21.6604279770704i	**−102.7506482038**71 +**21.660427977070**1i	**−102.7506482038**73 +**21.6604279770**684i
$Y_\nu(z)$ with $\nu = 30 + 50i$			
z	Reference	MATLAB `igamma`	Godfrey
70	−6.21989546226278 × 10^{23} +5.93644837574622 × $10^{23}i$	**−6.21989546226**806 × 10^{23} **+5.93644837574**486 × $10^{23}i$	**−6.21989546226**825 × 10^{23} **+5.93644837574**481 × $10^{23}i$
31	−2.04157148369613 × 10^{15} −9.38713109974277 × $10^{15}i$	**−2.04157148369613** × 10^{15} **−9.387131099742**98 × $10^{15}i$	**−2.04157148369**597 × 10^{15} **−9.38713109974**313 × $10^{15}i$
30	−3.54953866450241 × 10^{15} +1.95359736621662 × $10^{15}i$	**−3.549538664502**50 × 10^{15} **+1.9535973662166**3 × $10^{15}i$	**−3.549538664502**58 × 10^{15} **+1.953597366216**59 × $10^{15}i$
10	21.6604626085221 +102.750609923256i	**21.66046260**98798 **+102.75060992**2708i	**21.66046260**98782 **+102.75060992**2709

Table S1: Numerical values of Bessel functions $J_\nu(z)$ and $Y_\nu(z)$ calculated by three different algorithms. Bolded numbers indicate the consistent digits with the reference.